American Journal of Mechanical Engineering, 2016, Vol. 4, No. 2, 71-81
Available online at http://pubs.sciepub.com/ajme/4/2/5

DOI:10.12691/ajme-4-2-5

The Extension of the Q_L Method to Solve the Radiative Heat Transfer Problem in a 3D Square Enclosure Containing Non-grey Gas

Pedram Tazraei*

Department of Mechanical Engineering, Texas A&M University, College Station, TX 77840, USA
*Corresponding author: p.tazraei1@gmail.com

Abstract As a part of a general code for modeling behavior of combustion products, radiative heat transfer in non-grey and absorbing-emitting media is numerically investigated. The code is provided based on a new approach. A new method for solving the radiative transfer equation, called the Q_L method, is extended to 3D problems in non-grey media. There is also a discussion about the number of integration points of this method. A combination of the Q_L method, FT*n* FVM, CLAM scheme and SLW model was used to solve the radiative transfer equation. The results of the five test cases in 1-, 2- and 3D geometries containing water vapor and/or carbon dioxide are reported in this article. In all cases, the gas was non-isothermal and/or non-homogeneous. The accuracy of the method was assessed by benchmarking the results against previously published results where other methods were used and also against the outcome of employing Q_L method with the classical FVM, STEP scheme and SLW model. Also the cost of the presented method is compared with the results of combining FVM with the SLW model. The predictions by this method were found to be accurate and computationally cheaper. Therefore the results can be used in general code with full reliability.

Keywords: *radiative heat transfer, non-grey media, Q_L method, FTn FVM, SLW model, three dimensional*

Cite This Article: Pedram Tazraei, "The Extension of the Q_L Method to Solve the Radiative Heat Transfer Problem in a 3D Square Enclosure Containing Non-grey Gas." *American Journal of Mechanical Engineering*, vol. 4, no. 2 (2016): 71-81. doi: 10.12691/ajme-4-2-5.

1. Introduction

In many engineering applications, radiation is either the dominant mode of heat transfer or at least its contribution in overall heat transfer cannot be neglected. Specifically, radiation heat transfer in gases has been an interesting topic for thermal engineers due to its importance in atmospheric media and combustion systems, such as furnaces and combustors. Gaseous CO_2 and H_2O are the main products of fossil fuels, which also participate in radiative heat transfer.

Usually the radiative transfer equation (RTE) has to be solved for evaluating two important parameters in heat transfer, namely radiative heat flux on the surfaces and the radiative source term. Computational cost and accuracy of the applied method are key parameters to determine the RTE method of solution.

So far various numerical methods have been proposed for solving the RTE which are classified into two general groups. One group includes methods based on discretization of the radiative transfer equation such as the discrete ordinate method (DOM) [1], finite-volume method (FVM) [2,3], and finite element method (FEM) [4,5]. The other encompasses methods based on ray-tracing technique such as the Monte Carlo method [6] and zonal method [7]. In recent years, the the first group of methods have been attractive to the researchers because of their advantages, such as being flexible to handle complex geometry in multidimensional problems, over the ray tracing-based methods. A Comprehensive review on the development of various solution methods of RTE can be found in Modest [8] and Siegel and Howell [9]. Among these methods, finite volume and discrete ordinates methods have been widely used in problems of porous media [10,11], combustion applications [12], furnace design [13], curvilinear coordinates [14], irregular geometries [15], etc. In addition to being consistent with other numerical techniques used in determining the flow and temperature fields, this method has other merits such as being easily programmable, fairly accurate and computationally cheap. However, applying these methods is accompanied with two major drawbacks due to discretizing the spatial and angular domains; i.e. false scattering and ray effect. Therefore the attempt for testing and improving these methods to achieve higher accuracy and lower computational time has been going on since their evolution [16-26]. Although these two effects are not independent of each other [19], in general, false scattering is attributed to spatial discretization and finer grids can mitigate this undesirable effect. Li [21] suggested a hybrid spatial scheme to lessen the false scattering in DOM. Chai [22] and Chai et al. [11] have concluded that the FVM with CLAM schemes gives more accurate results than FVM with the STEP scheme in 2- and 3-D geometries.

The angular discretization is responsible for the ray effect. Coelho [23] proposed a modified version of DOM which was able to reduce the ray effect caused by abrupt changes in medium or wall temperatures. The same author [25] compared various spatial discretization schemes of RTE. He concluded that although the CLAM scheme [28] is not the most accurate one, it can be perceived as the most efficient scheme considering the trade-off between accuracy and calculation time. Baek et al. [26] combined the FVM and Monte Carlo method and showed favorable decreases in the ray effect. FT*n* FVM was proposed by Kim and Huh [27]. They utilized a new angular discretization for 3-D radiative heat transfer problems. They demonstrated that the ray effect becomes less by using this angular grid in comparison with classical FVM. Together with the CLAM scheme, FT*n* FVM was successfully used in radiative problem in non homogeneous media and the irregular geometries of combustion chambers [29,30].

The Q_L method, which was proposed by Hassanzadeh et al. [31], Hassanzade and Raithby [32] and Hassanzadeh [33], has been proved by Moghadassian et al. [34] to be very accurate, computationally cheap and flexible enough to handle the problems where radiation is not the only heat transfer mode. The aim of this method is to combine the high accuracy of the methods for finding directional radiative intensities (like FVM and DOM) with the speed of simpler methods like P_1. This goal has been achieved by defining the concept of phase weight. Numerous problems in 1- and 2-D grey, emitting, absorbing and scattering media have been solved by the founders of this method and the method was shown as an excellent new technique for solving RTE [33] . High convergence speed was achieved by the Q_L method, especially in optically thick media where methods like FVM fail to behave appropriately. Moreover, the method was found accurate and fast in handling direct and inverse radiation- natural convection problems [34,35]. This speed in convergence fully compensates for the additional calculation of this method in modeling the physical phenomena.

The assumption of grey media is less likely true as far as radiation in gases is considered; therefore, one of the important issues in gas radiation is the description of the radiative properties of non-grey gases. Various models to define gas properties can be roughly sorted in three groups: 1) spectral line-by-line, 2) spectral band models and 3) global models. The complexity of the models decreases from group (1) to (3). Although line-by-line models are so precise, they have just been used as references due to their enormous computational requirements. Band models (like SNB and WBM) have not been utilized so often because of their computational burden and/or incompatibility with famous RTE solvers like FVM [8,14]. Instead, global methods like WSGG and LSW have been usually preferred by researchers due to their efficiency. The WSGG model was initially developed by Hottel and Sarofin [36]. Modest [37] showed that WSGG model can be linked with any RTE solution method. This model was coupled with the discrete ordinates and the discrete transfer methods [38,39] for radiation assessment. However, severe temperature gradients may cause this model to yield erroneous results, higher than 30%, as discussed by Soufiani et al [38]. Based on the general concept of WSGG, Denison and Web developed the SLW model [40]. They continued their work to formulate parameters of the model in non-homogenous and/or non-isothermal medium containing H_2O and/or CO_2 [41,42,43,44]. This model is widely used to find real gas properties [45-52] and some authors like Goutiere et al. [50] and Coelho [51] and Çayan and Selçuk [52] claimed that it is the most efficient model which gives relatively accurate results in a short calculation time.

The aim of this study is to extend the Q_L method to 3-D non-grey media and present a technique for solving RTE by combining the Q_L and FT*n* FV methods with the CLAM scheme and SLW model. Eight different cases with different dimensionalities were solved by this technique and compared with previous models. For all cases good agreement has been observed. But for the sake of conciseness, just five of the cases, which represent the more complex ones, are reported in this article.

2. Mathematical Formulation

2.1. Radiative Transfer Equation (RTE)

The radiative transfer equation for each grey gas i in non-grey, emitting and absorbing medium is

$$\frac{dI_i^l}{ds} = \kappa_i \left[a_i I_b - I_i^l \right] \tag{1}$$

with the following condition for grey boundary

$$I_{i,wall}^l = \varepsilon\, a_i I_{b,wall} + \frac{1-\varepsilon}{\pi} \sum_{l'} I_{i,wall}^{l'} X_{wall}^{l'} \tag{2}$$

where

$$X_{wall}^l = \int_{\omega^l} \mathbf{s}\cdot\mathbf{n}_{wall}\, d\omega,\ \ d\omega = \sin\theta\, d\theta\, d\phi \tag{3a}$$

$$\begin{aligned} \mathbf{s} &= s_1\mathbf{e}_1 + s_2\mathbf{e}_2 + s_3\mathbf{e}_3 = \\ &= \sin\theta\cos\phi\,\mathbf{e}_1 + \sin\theta\sin\phi\,\mathbf{e}_2 + \cos\theta\,\mathbf{e}_3 \end{aligned} \tag{3b}$$

The net radiative heat flux at wall is

$$q_{wall} = \varepsilon \left(\sum_i^{N_g} \sum_{l'} I_{i,wall}^l \omega^l N_{wall}^l - a_i \pi I_{b,wall} \right) \tag{4}$$

And radiative source term is

$$\nabla\mathbf{q} = 4\pi \sum_i^{N_g} \kappa_i \left(a_i I_{b,wall} - I_{a,i} \right) \tag{5}$$

The aim of this study is to extend the works of Hassanzadeh [33] and Moghadassian et al. [34] to combine the Q_L method with FT*n* FVM to solve the RTE. Also a high resolution CLAM scheme is deployed to relate facial and nodal intensities. The detailed solution procedure is coveredt in the appendix. In addition, non-grey behavior of the gas is predicted by the SLW model.

2.2. SLW Model

The SLW model provides the values of κ_i and a_i. The mathematical background of this model can be found elsewhere [40]. Here a brief formulation is presented.

To start, suppose that only one species of an isothermal and homogenous participating gas (H_2O or CO_2) is in the enclosure. The absorption cross-section domain is divided to N_g logarithmically equally spaced bands. Now consider the i-th band. In this band the absorption cross section is between two successive supplemental absorption cross-sections namely $\hat{C}_{abs,i}$ and $\hat{C}_{abs,i+1}$. Then κ_i and a_i are calculated by the following formulas.

$$\begin{aligned}\kappa_i &= NC_{abs,i} \text{ and}\\ a_i &= F_s\left(\hat{C}_{abs,i+1},T_b,T_g,p_T,Y_s\right)\\ &\quad -F_s\left(\hat{C}_{abs,i},T_b,T_g,p_T,Y_s\right)\end{aligned} \tag{6}$$

where

$$C_{abs,i}=\exp\left[\frac{\ln\left(\hat{C}_{abs,i}\right)+\ln\left(\hat{C}_{abs,i+1}\right)}{2}\right] \tag{7}$$

The values of F_s can be derived from a HITRAN database [53]. However, in this study the correlations for calculating F_s for H_2O and CO_2 given in [43,44] are used. When two gases are in the enclosure simultaneously, the absorption cross-section domain of each gas is divided to N_g bands separately. If i and j denote the i-th band of the absorption cross-section domain of H_2O and j-th band of the absorption cross-section domain of CO_2, respectively; κ and a must be calculated for each combination of i and j.

$$\kappa_{i,j}=N_{H_2O}C_{abs,i}+N_{CO_2}C_{abs,j} \quad \text{and} \quad a_{i,j}=a_i\times a_j \tag{8}$$

Then these vales replace κ_i and a_i in Eq. (1) and this equation must be solved for each combination of i and j.

Additional treatment is needed for the general case of non-isothermal and/or non-homogenous medium. In this case Eq. (8) is no longer valid and $C_{abs,i}$ has to be calculated locally. The following implicit equation must be solved by trial and error to give the value of local $C_{abs,i}$.

$$\begin{aligned}&F_s\left(\begin{matrix}C_{abs,i},T_b=T_{ref},T_g=T_{loc},\\ p_T=p_{T,loc},Y_s=Y_{s,loc}\end{matrix}\right)\\ &=F_s\left(\begin{matrix}C_{abs,i,ref},T_b=T_{ref},T_g=T_{ref},\\ p_T=p_{T,ref},Y_s=Y_{s,ref}\end{matrix}\right)\end{aligned} \tag{9}$$

Where T_{ref}, $P_{tot,ref}$ and $Y_{s,ref}$ are the spatial average of the local values of these parameters and $C_{abs,ref}$ is calculated by Eq. (9). Then Eq. (8) is locally applied.

$$\begin{aligned}\kappa_j &= N\left(T_{loc},p_{T,loc},Y_s=Y_{s,loc}\right)\times\\ &\quad C_{abs,i}\left(T_{loc},p_{T,loc},Y_s=Y_{s,loc}\right)\end{aligned} \tag{10a}$$

$$\begin{aligned}a_i &= F_s\left(\begin{matrix}\hat{C}_{abs,i+1},T_b,T_g=T_{ref},\\ p_T=p_{T,ref},Y_s=Y_{s,ref}\end{matrix}\right)\\ &\quad -F_s\left(\begin{matrix}\hat{C}_{abs,i},T_b,T_g=T_{ref},\\ p_T=p_{T,ref},Y_s=Y_{s,ref}\end{matrix}\right)\end{aligned} \tag{10b}$$

where T_b equals T_{loc} for inside the domain or T_{wall} on the walls. The reader is referred to [41] to find complete information about the non-isothermal and/or inhomogenous case. In this study N_g=15 and the absorption cross section domain for water is between 3×10^{-5} and 60 mol/m^2 and for carbon dioxide it is between 3×10^{-5} and 120 mol/m^2; The ideal gas assumption is considered to obtain the value of molar density; the non-participating gas is N_2; p_{tot}=1 atm and theNewton-Raphson method is used for the iterative solution of Eq. (9) whenever needed.

3. Results and Discussion

The five test cases are considered. The results of employing Q_L with FTn FVM and CLAM scheme are compared against previously published results. The details of Q_L method can be found in the Appendix.

3.1. Test Case 1

In this case, the radiative heat transfer occurs between two infinite parallel cold black surfaces at 0K. The medium between the two surfaces is filled with non-grey gas at 1000K. The mole fraction of H2O is varying with a parabolic function which has the value of 0 at walls and reaches its peak (100%) at the centerline. This problem is solved by Denison and Webb [41] with the assumptions of spatially constant medium (not using Eqs. (10a) and (10b)) and taking the spatial effect (using Eqs. (10a) and (10b)). The results of both assumptions as well as the predicted results of this study are shown in Figure 1. Very good agreement is seen between present results and previously reported ones.

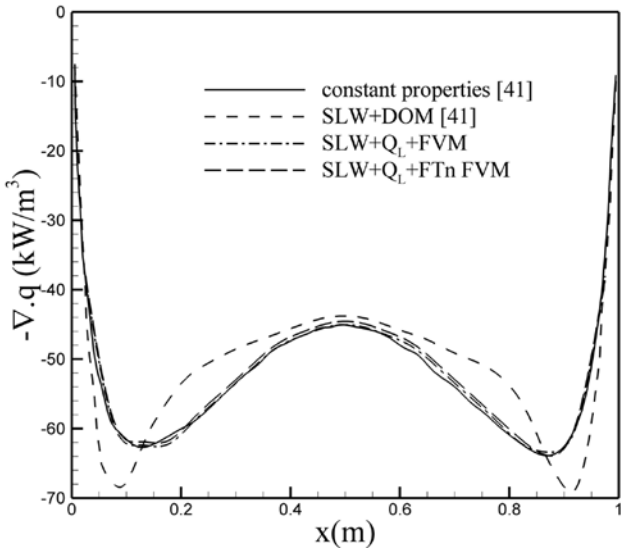

Figure 1. Result of the first case: the radiative source term between two infinite parallel surfaces

3.2. Test Case 2

This time the radiative heat transfer in a 2-D square enclosure is considered. The 1m×0.5m enclosure of Figure 2a is studied. Non-isothermal and non-homogenous H_2O is the only participating gas inside the enclosure whose temperature and concentration varies according to

$$\begin{aligned}&T(x,y)\\ &=T_0\left[0.3333\left(1-2\left|x-0.5\right|\right)\left(1-4\left|y-0.25\right|\right)+1\right]\\ &Y(x,y)=Y_0\left[4\left(1-2\left|x-0.5\right|\right)\left(1-4\left|y-0.25\right|\right)+1\right]\end{aligned} \tag{11}$$

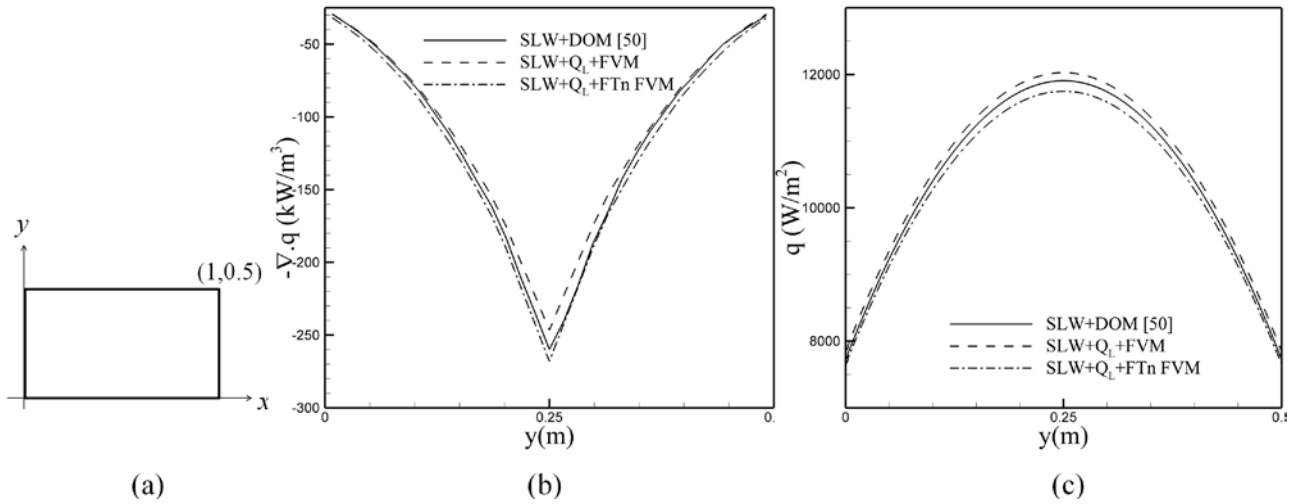

Figure 2. (a) The geometry of the second and third test cases and (b) the radiative source term along the midsection of the enclosure for the second case and (c) the radiative flux on the left wall of the enclosure for the second case

The heat flux on the left wall and the radiative source term along the midsection of the enclosure (x=0.5m) are compared with the results of Goutiere et al. [50]. This comparison is seen in Figure 2b and Figure 2c. The source term has a V-shaped distribution. It is lower near the walls because the temperature and the optical thickness of the medium are lower. At a further distance from the wall, the absolute value of the source term becomes increasingly important due to the rapid increase in temperature and concentration, and reaches a very high value at the peak temperature in the middle of the enclosure, where the emitted energy density is significantly higher than the absorbed radiant energy density. In addition, the heat flux has its lowest value at the ends of the centerline because of lower heat transfer due to the lower temperature and optical thickness of the gas. Also the presence of cold walls (bottom and top walls) has a great influence on the heat flux of the left wall. By rising, the effect of these walls diminishes and the radiative heat flux is enhanced.

3.3. Test Case 3

This case is similar to the previous case except that a mixture of 10 % CO_2 and 20% H_2O is the non-grey gas. The temperature field in the medium varies according to

$$\begin{aligned} &for\ x \le 0.1 : T(x,y) \\ &= (14000x - 400)\left(1 - 3y_0^2 + 2y_0^3\right) + 800 \\ &for\ x > 0.1 : T(x,y) \\ &= -\frac{10000}{9}(x-1)\left(1 - 3y_0^2 + 2y_0^3\right) + 800 \end{aligned} \tag{12}$$

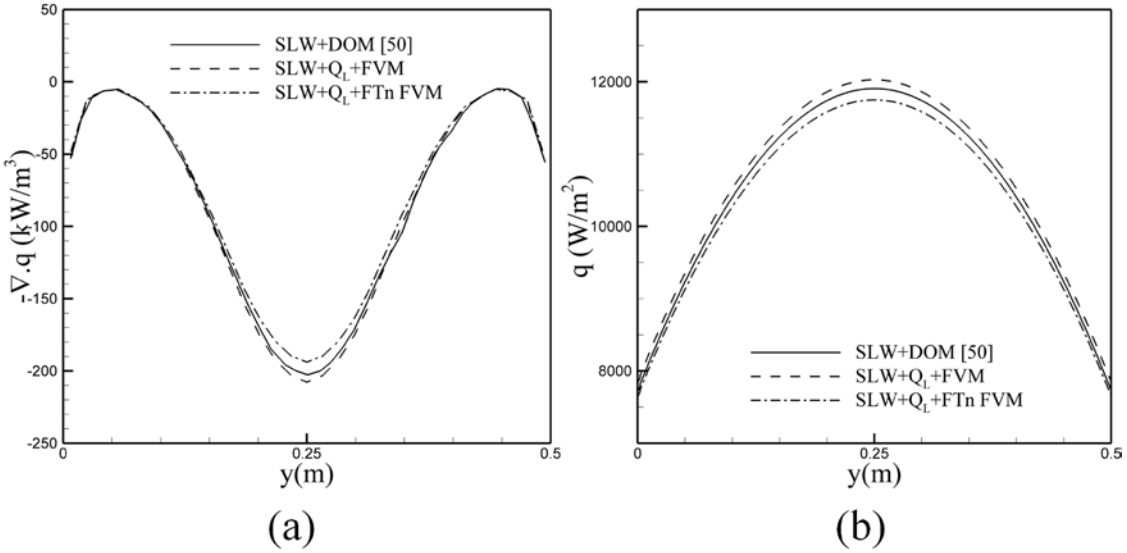

Figure 3. Results of the third case (a) the radiative source term along the midsection of the enclosure and (b) the radiative flux on the left wall of the enclosure

Again, the heat flux on the left wall and the radiative source term along the midsection of the enclosure (x=0.5m) are compared with the results of Goutiere et al. [50] as shown in Figure 3a and Figure 3b. As can be seen, the radiative source term has an M-shaped distribution. The negative slope of the source term distribution near the walls is due to the variation of the optical depth along the centerline, which is low near the walls and high in the middle. The cells adjacent to the walls emit more energy to the cold surfaces than they receive from the hot regions. At further distances from the walls, the effect of the cold regions lessens, thus leading to a lower absolute value of

the source term. As stated in the previous case, by moving further along the centerline, the absolute value of the source term becomes higher due to the enhancement of temperature and concentration, and reaches its peak in the middle of the enclosure. Both heat flux and source term are symmetric along the y-direction due to the symmetry of the temperature field and boundary conditions relative to this direction.

3.4. Test Case 4

This test case is a rectangular enclosure of 2m×2m×4m containing emitting, absorbing and non-scattering gases surrounded by black walls at 300 K. The gas is a non-homogenous mixture of N_2 and H_2O at 1000K. The mole fraction of H_2O varies with the height according to z-$0.25z^2$. The same problem is considered by Selçuk and Doner [49]. The comparison between the results of the present study with the previous works is demonstrated in Figure 4a and Figure 4b. It is seen that the radiative source term is much higher near the walls due to the temperature difference between the gas and cold walls. But at further distances, the effect of the cold walls is reduced and due to the presence of an isothermal gas, the absolute value of radiative source term reduces. The initial negative slope of the radiative source term of Figure 4a can be explained by the same reasoning as the previous case.

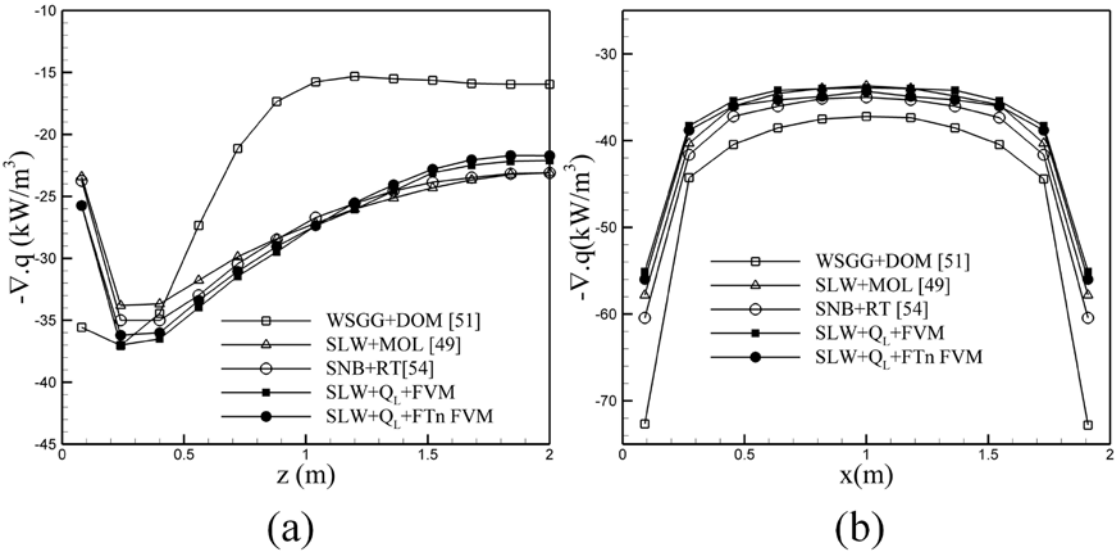

Figure 4. Results of the forth case; the radiative source term along (a) along the centerline (x=1m, y=1m, z) and (b) along (x, y=1m, z=0.24m)

3.5. Test Case 5

The radiative heat transfer in a non-isothermal and homogenous mixture of 10% CO_2 and 20% H_2O in the same rectangular enclosure of the previous case is considered. The temperature in the enclosure varies according to $T=(T_c-T_e)\ f(r/R)+T_e$ where T_c is the temperature of the centerline (x=1m, y=1m, z) and T_e=800K is the temperature of the exiting gas at z=4m. Where T_c is assumed to increase linearly from the temperature of the entering gas at z=0 (400K) to 1800K at z=0.375m and then decrease linearly to a value of 800K at exit (z=4m). r is the distance from the centerline and $f(r/R)=1-3(r/R)^2+2(r/R)^3$ in which R=1m. The gas temperature outside the cylindrical region is assumed to be uniform at 800K. All walls are black at 300K. This case was previously studied [49].

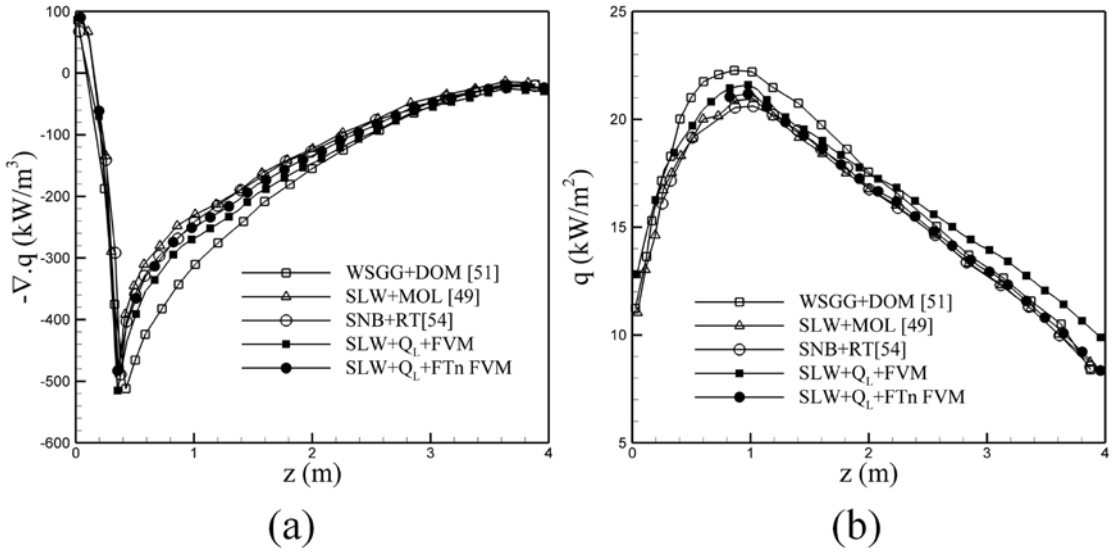

Figure 5. Results of the fifth case (a) the radiative source term along the centerline (x=1m, y=1m, z) and (b) the radiative flux along the line (x=2m, y=1m, z)

In Figure 5a and Figure 5b the comparison between the radiative source term and radiative heat flux with the previous works is shown. The radiative heat flux is asymmetric along the z direction due to the asymmetric variation of T_c along this coordinate. Also it has a higher value relative to the previous case due to a larger temperature difference. Similar to the previous cases, a negative slope in the diagram of radiative source term is seen. The absolute value of the radiative source term occurs at around z=0.375m where T_c reaches its maximum. But the occurrence of the maximum value of the radiative flux is delayed until z=1m because of the influence of the cold walls.

As can be seen, in all cases a good agreement between the results of the present study and those of the previous works exist. It can be deduced that the present algorithm has enough accuracy to be applied in cases of non-grey media.

Although the reduction of time by using the Q_L method instead of FVM is more noticeable for grey gas [31,32,33], the Q_L method is still found less time consuming when compared to FVM. For non-grey cases the typical value of $t_{tot,QL}/t_{tot,FVM}$ where t_{tot} is the total computational time, is between 0.75-0.9. The ratio is relatively high in comparison with grey cases as reported by Hassanzadeh [33]. For non-grey cases, most of the calculation time is devoted to find the non-grey gas parameters. Therefore the reduction in calculation time is not remarkable. It is especially true for the cases of non-grey mixture (relative to the cases of single non-grey species) where SLW model is computationally very demanding ($t_{tot,QL}/t_{tot,FVM}$ is around 0.9).

4. Conclusions

In this work the Q_L method, which is a recent method for solving the radiative transfer equation, is extended to three dimensional geometries filled with non-grey gas. The FT*n* finite volume method is used to get the directional intensities and the CLAM scheme is used to relate the facial intensities to the nodal values. It is found that the accuracy of the method is preserved even with fewer integration points. Moreover, five different cases of non-homogenous and non-isothermal gas are considered. The SLW model is used to predict the behavior of non-grey gas. It is found that the new approach can be utilized in non-grey media with high accuracy. However, the reduction in the computational time is not as pronounced as reported for the grey cases.

References

[1] Fiveland, W.A., "Three-dimensional radiative heat-transfer solutions by the discrete-ordinates method," *J Thermophys Heat Transfer*, 2, 309-316, 1988.

[2] Raithby, G.D. and Chui, E.H., "A finite-volume method for predicting a radiant heat transfer in enclosures with participating media," *J Heat Transfer*, 112, 415-423, 1990.

[3] Chai, J.C. and Lee, H.S., "Finite-volume method for radiation heat transfer," *J Thermophys Heat Transfer*, 8, 419-25, 1994.

[4] Kisslelev, V.B., Roberti, L. and Perona G., "An application of the finite-element method to the solution of the radiative transfer equation," *J Quant Spectrosc Radiat Transfer*, 51, 603-614, 1994.

[5] Liu, L.H., "Finite element simulation of radiative heat transfer in absorbing and scattering media," *J Thermophys Heat Transfer* 18, 555-567, 2004.

[6] Howell, J.R. and Perlmutter, M., "Monte Carlo solution of thermal transfer through radiant media between gray walls," *J Heat Transfer*, 86, 116-222, 1964.

[7] Hottel, H.C. and Cohen, E.S., "Radiant heat exchange in a gas-filled enclosure allowance for nonuniformity of gas temperature," *AIChE J*, 4, 3-14, 1958.

[8] Modest, M.F., *Radiative Heat Transfer*. 2nd ed, Academic Press, New York, 2003.

[9] Siegel, R. and Howell, J.R., *Thermal Radiation Heat Transfer*. 3rd ed. Hemi-sphere Publishing Corp., 1992.

[10] Kowsary, F., Gholamian, H., Ashjaee, M. and Moghadassian,B., "Inverse identification of radiative properties of a multi-component media in MPA modeling of radiative transfer," *International Communications in Heat and Mass Transfer*, 95-105, 2016.

[11] Kowsary, F., Gholamian, H. and Moghadassian, B., "On the sensitivity of surface reflectance to specularity and phase function parameters in MPA modeling of radiative transfer in two-component media." *Numerical Heat Transfer, Part B: Fundamentals* 1-17, 2015.

[12] Coelho, P.J., Teerlinga, O.J. and Roekaerts, D. "Spectral radiative effects and turbulence/radiation interaction in a non-luminous turbulent jet diffusion flame," *J Combust Flame*, 133, 75-91, 2003.

[13] Moghadasian, M. and Moghadassian, B. "3D Inverse Boundary Design Problem of Conduction-radiation Heat Transfer," *Journal of Applied Sciences*, 12, 233, 2012.

[14] Talukdar, P., Steven, M., Issendroff, F.V. and Trimis, D. "Finite volume method in 3-D curvilinear coordinates with multiblocking procedure for radiative transport problems," *Int J Heat Mass Transfer* 48, 4657-66, 2005.

[15] Jafari, A., Rahimian M.H. and Saeedmanesh. A., "An unsteady mixed convection in a driven cavity filled with nanofluids using an externally oscillating lid." *Journal of Electronics Cooling and Thermal Control* 3.02, 58, 2013.

[16] Shokouhmand, H., Noori Rahim Abadi S.M.A., and Jafari, A. "The effect of the horizontal vibrations on natural heat transfer from an isothermal array of cylinders." *International Journal of Mechanics and Materials in Design* 7.4, 313-326, 2011.

[17] Chai, J.C., Lee, H.S. and Patankar, S.V., "Treatment of irregular geometries using a Cartesian coordinates finite-volume radiation heat transfer procedure," *Numer Heat Transfer, Part B*, 26, 225-35, 1994.

[18] Chai, J.C., Lee, H.S. and Patankar, S.V., "Ray effect and false scattering in the discrete ordinates method," *Numer Heat Transfer Part B*, 24, 359-73, 1993.

[19] Raithby, G.D., "Evaluation of discretization errors in finite-volume radiant heat transfer predictions," *Numer Heat Transfer Part B*, 36, 241-264, 1999.

[20] Malvandi, A., Moshizi, S. A., and Ganji, D. D., "Effect of Magnetic Fields on Heat Convection Inside a Concentric Annulus Filled with Al2O3–water Nanofluid," *Adv. Powder Technol*., 25, 1817-24, 2014.

[21] Li, H.S., "Reduction of false scattering in arbitrarily specified discrete directions of the discrete ordinates method," *J Quant Spectrosc Radiat Transfer*, 86, 215-22, 2004.

[22] Chai, J.C., "Transient radiative transfer in irregular two-dimensional geometries," *J Quant Spectrosc Radiat Transfer*, 84, 281-94, 2004.

[23] Coelho, P.J., "Bounded skew high-order resolution schemes for the discrete ordinates method," *J Comput Phys*, 175:412-37, 2002.

[24] Schobeiri, M. T., and Nikparto, A., "A comparative Numerical Study of Aerodynamics and Heat Transfer on Transitional Flow Around a Highly Loaded Turbine Blade with Flow Separation Using RANS, URANS and LES," ASME Turbo Expo 2014: Turbine Technical Conference and Exposition. American Society of Mechanical Engineers, 2014.

[25] Coelho, P.J., "A comparison of spatial discretization schemes for differential solution methods of the radiative transfer equation," *J Quant Spectrosc Radiat Transfer*, 109, 189-200, 2008.

[26] Baek, S.W., Byun, D.Y., and Kang, S.J., "The combined Monte-Carlo and finite-volume method for radiation in a two-dimensional irregular geometry," *Int J Heat Mass Transfer*, 43, 2337-44, 2000.

[27] Kim, S.H. and Huh, K.Y., "A new angular discretization scheme of the finite volume method for 3-D radiative heat transfer in

absorbing, emitting and anisotropically scattering media," *Int J Heat Mass Transfer*, 43, 1233-42, 2000.

[28] Van Leer, B., "Towards the ultimate conservation difference scheme. II. Monotonicity and conservation combined in a second-order scheme," *J Comput Phys*, 14, 361-70, 1974.

[29] Kamel, G., Naceur, B.M., Rachid, M. and Rachid, S., "Formulation and testing of the FT*n* finite volume method for radiation in 3-D complex inhomogeneous participating media," 98, 425-45, 2006.

[30] Borjini, M.N., Guedri, K. and Saïd, R. "Modeling of radiative heat transfer in 3D complex boiler with non-gray sooting media," *J Quant Spectrosc Radiat Transfer*, 105, 167-79, 2007.

[31] Hassanzadeh, P., Raithby, G.D. and Chui, E.H. "The efficient calculation of radiation heat transfer in participating media," *J Thermophys Heat Transfer*, 22, 129-39, 2008.

[32] Hassanzadeh, P. and Raithby, G.D., "The efficient calculation of radiation heat transfer in anisotropically scattering media using the Q_L method.," *J Comput Thermal Sci*, 1, 189-206, 2009.

[33] Hassanzadeh, P. "An efficient computational method for thermal radiation in participating media," PhD thesis, University of Waterloo, Canada, 2007.

[34] Moghadassian, B., Kowsary, F. and Gholamian, H., "Natural Convection-Radiation Heat Transfer in Rectangular Cavity With the Presence of Participating Media." *ASME 2010 10th Biennial Conference on Engineering Systems Design and Analysis*. American Society of Mechanical Engineers, 2010.

[35] Moghadassian, B., and Kowsary, B., "Inverse boundary design problem of natural convection–radiation in a square enclosure." *International Journal of Thermal Sciences*, 75, 116-26, 2014.

[36] Hottel, H.C. and Sarofim, A.F. *Radiative Transfer*. McGrawHill, New York, 1967.

[37] Modest, M.F., "The weighted-sum-of-gray-gases model for arbitrary solution methods in radiative transfer," *ASME J Heat Transfer*, 113, 650-56, 1991.

[38] Soufiani, A. and Djavdan, E., "A comparison between weighted sum of gray gases and statistical narrow-band radiation models for combustion applications," *J Combust Flame*, 97, 240-50, 1994.

[39] Bressloff, N.W., Moss, J.B. and Rubini, P.A., "CFD Prediction of coupled radiation heat transfer and soot production in turbulent flames," In Proceedings of 26th International Symposium on Combustion, 2379-86, The Combustion Institute, Pittsburgh, USA, 1996.

[40] Denison, M.K. and Webb, B.W. "A spectral line-based weighted-sum-of-gray-gases model for arbitrary RTE solvers," *ASME J Heat Transfer*, 115, 1004-12, 1993

[41] Denison, M.K. and Webb, B.W., "The spectral line-based weighted-sum-of-gray-gases model in non-isothermal non-homogeneous media," *ASME J Heat Transfer*, 117, 359-65, 1995.

[42] Denison M.K. and Webb, B.W., "The spectral line weighted-sum-of-gray-gases model for H_2O/CO_2 mixture," *ASME J Heat Transfer*, 117, 788-92, 1995.

[43] Denison, M.K. and Webb, B.W., "An absorption-line blackbody distribution function for efficient calculation of total gas radiative heat transfer," *J Quant Spectrosc Radiat Transfer*, 50, 499-510, 1993.

[44] Denison, M.K. and Webb, B.W. "Development and application of an absorption line blackbody distribution function for CO_2," *Int J Heat Mass Transfer*, 38, 1813-21, 1995.

[45] Moghadassian, B., Kowsary, F. and Mosavati, M., "The Radiative Boundary Design of a Hexagonal Furnace Filled With Gray and Nongray Participating Gases," *Journal of Thermal Science and Engineering Applications*, 5(3), 031005, 2013.

[46] Solovjov, V.P. and Webb, B.W., "Multilayer modeling of radiative transfer by SLW and CW methods in non-isothermal gaseous medium," *J Quant Spectrosc Radiat Transfer*, 109, 245-57, 2008.

[47] Solovjov, V.P. and Webb, B.W., "SLW modeling of radiative transfer in multicomponent gas," *J Quant Spectrosc Radiat Transfer*, 65, 655-72, 2000.

[48] Solovjov, V.P. and Webb, B.W. "Application of CW local correction approach to SLW modeling of radiative transfer in non-isothermal gaseous media," *J Quant Spectrosc Radiat Transfer*, 111, 318-24, 2010.

[49] Selçuk, N. and Doner, N., "A 3-D radiation model for non-grey gases," *J Quant Spectrosc Radiat Transfer*, 110, 184-91, 2009.

[50] Goutiere, V., Liu, F. and Charette, A., "An assessment of real-gas modelling in 2D enclosures," *J Quant Spectrosc Radiat Transfer*, 64, 299-26, 2000.

[51] Coelho, P.J., "Numerical simulation of radiative heat transfer from non-gray gases in three-dimensional enclosures," *J Quant Spectrosc Radiat Transfer*, 74, 307-28, 2002.

[52] Çayan, F.N. and Selçuk, N., "A comparative study of modeling of radiative heat transfer using MOL solution of DOM with gray gas, wide-band correlated-*k*, and spectral line-based weighted sum of gray gases models," *Numer Heat Transfer Part B*, 52, 281-96, 2007.

[53] Rothman, L.S., Gamache, R.R., Tipping, R.H., Rinsland, C.P., Smith, M.A.H. and Benner, D.C. et al., "The HITRAN molecular database: editions of 1991 and 1992a," *J Quant Spectrosc Radiat Transfer*, 48, 469-507, 1992.

[54] Liu, F., "Numerical solutions of three-dimensional non-grey gas radiative transfer using the statistical narrow-band model," *Trans ASME*, 121, 200-203, 1999.

Appendix A

The $\mathbf{Q}_L$ method was originally derived for a 2-D grey media [33]. The extension to 3-D non-grey media is done here by integrating the RTE (Eq. (1)) over a control volume and a control angle and applying Gauss divergence theorem. The left side is

$$\int_{4\pi}\int_{V_p}\frac{dI^l}{ds}dVd\omega=\int_{4\pi}\int_{V_p}\nabla\cdot\left(I^l\mathbf{s}\right)dVd\omega = \int_{A_{s,p}}\left[\int_{4\pi}I^i\mathbf{s}d\omega\right]\cdot\mathbf{n}dA_s \tag{A.1}$$

The radiant heat flux is

$$q(\mathbf{r})=\int_{4\pi}I^l(\mathbf{r})\mathbf{s}d\omega \tag{A.2}$$

Combining Eqs. (A.3) and (A.4) will give

$$\int_{4\pi}\int_{V_p}\frac{dI^l}{ds}dVd\omega=\int_{A_{s,p}}q(\mathbf{r})\cdot\mathbf{n}dA_s \tag{A.3}$$

And by equaling integration of left and right sides of RTE the following equation (known as radiative energy equation REE) is derived

$$\int_{A_{s,p}}q(\mathbf{r})\cdot\mathbf{n}dA_s=4\pi\int_{V_p}\kappa\left[aI_b-I_a\right]dV \tag{A.4}$$

where

$$I_a=\frac{1}{4\pi}\int_{4\pi}I^l d\omega \tag{A.5}$$

Rearranging RTE gives

$$I^l=aI_b-\frac{dI^l}{\kappa ds} \tag{A.6}$$

Replacing I^l from the above equation into Eq. (A.4) will give

$$q(\mathbf{r})=\frac{-1}{\kappa}\mathbf{I}_{tr} \tag{A.7}$$

The I_b term vanishes because

$$\int_{4\pi}\mathbf{s}d\omega=0 \tag{A.8}$$

And the transport integral is

$$\mathbf{I}_{tr} = \left[\int_{4\pi} \frac{\partial I^l}{\partial x_k} s_k s_j d\omega \right] \mathbf{e}_j \tag{A.9}$$

By definig the directional phase weight α^l as

$$\alpha^l = \frac{I^l}{I_a} \tag{A.10}$$

I_{tr} can be stated as

$$\begin{aligned} \mathbf{I}_{tr} &= \left[\frac{\partial}{\partial x_k} \int_{4\pi} I^l s_k s_j d\omega \right] \mathbf{e}_j \\ &= \frac{\partial}{\partial x_k} \left[I_a \sum_{l=1}^{L} \left(\alpha^l \int_{\omega^l} s_k s_j d\omega \right) \right] \mathbf{e}_j \end{aligned} \tag{A.11}$$

And by defining the following relation

$$T_{jk} = \sum_{l=1}^{L} \left[\alpha^l \int_{\omega^l} s_k s_j d\omega \right] \tag{A.12}$$

And combining Eqs. (A.5) and (A.9) the Q_L equation for non-scattering gas is obtained

$$\begin{aligned} &\sum_{ip} \left[\frac{\partial}{\partial x_k} \left(I_a T_{jk} \right) \right] \mathbf{e}_j \cdot \mathbf{n}_{ip} dA_{s,ip} \\ &= 4\pi\kappa^2 V_p \left[a I_b - I_{a,p} \right] \end{aligned} \tag{A.13}$$

In Figure A.1(a) a control volume with its representative node, P (marked by ● in the figure) and the corresponding integration points, marked by * in the figure, are shown. The $A_{s,ip}$ is the partial area of the control surface that is represented by *ip*-th integration point. For better visualization, the $A_{s,1}$ is illustrated in Figure A.1(a).

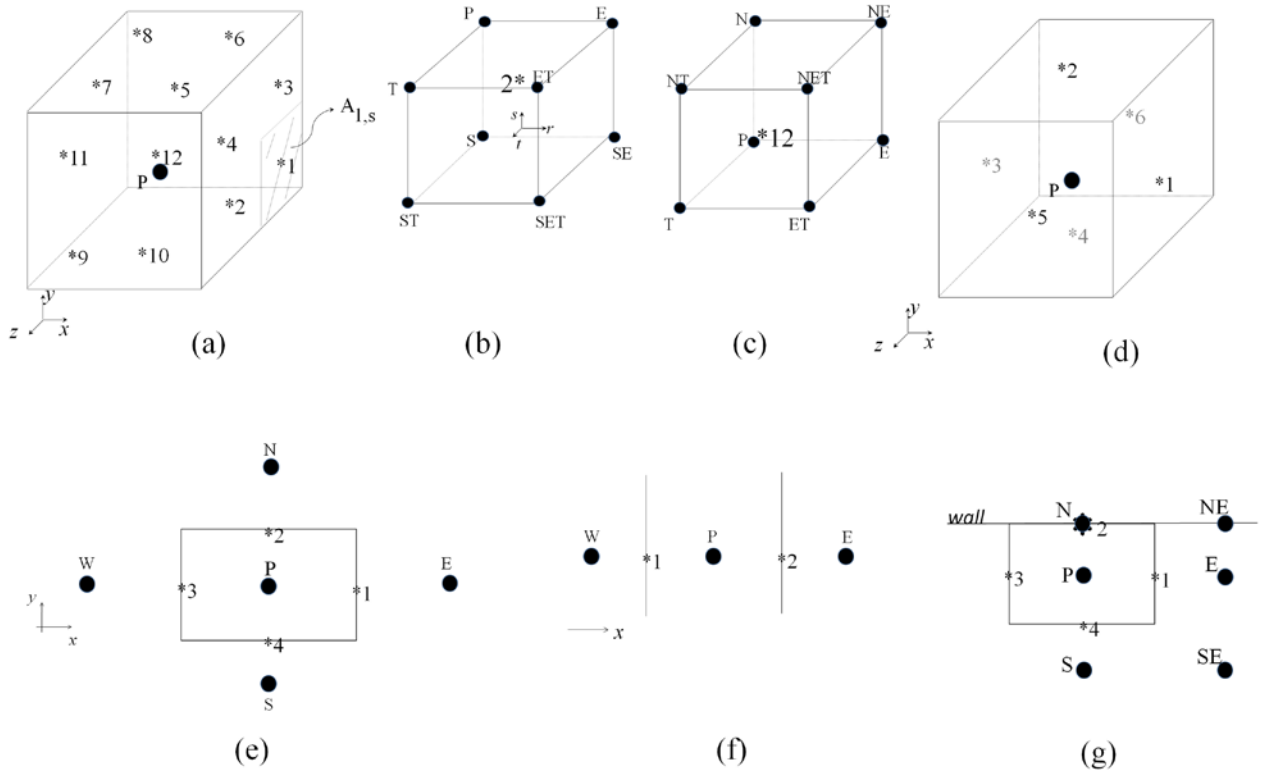

Figure A1. (a) A 3D control volume with 24 integration points, (b) neighbor nodal points and auxiliary coordinates around *ip*=2, (c) neighbor nodal points and auxiliary coordinates around *ip*=12, (d) a 3D control volume with 6 integration points, (e) a 2D control volume with 4 integration points, (f) a 1D control volume with 2 integration points and (g) a 2D boundary control volume

In general, the accuracy of the method increases when the total number of integration points increases. But a balance between the accuracy and computational cost must be considered. Moghadassian [34] studied the effect of the number of integration points on results of the Q_L method for the 2- and 3D radiative problem. He found that the optimal number of integration points is 6 for a 3-D element (1 on each side of the element) and 4 for a 2D element. But for illustrative purposes, a 3-D control volume with 24 integration points is shown in Figure A.1(a) and the equations are discretized for this control volume. There are 24 integration points for a 3-D control volume (4 on each side) but only those on visible sides, i.e. east, north and top sides, are shown for the sake of clarity. Assume that *W* is an arbitrary quantity. Then *W* at integration points is related to *W* at nodal points by assuming a linear profile in the 3-D corresponding element. The 3-D corresponding element is an enclosure where the neighbor nodes are its vertices. It is illustrated for *ip*=2 and *ip*=12 in Figure A.1(b) and Figure A.1(c). An auxiliary coordinate (*r*-*t*-*s*) is defined. *r*, *t* and *s* vary between [-1,1] in the cubic element and the derivatives are transferred to this new coordinates. Where *W* at any point inside the element of Figure A.1(b), for instance, can be related to the nodal values of *W* by the following linear relation:

$$W(r,t,s)=\frac{\begin{pmatrix}(1-r)(1-s)(1-t)W_S+\\(1-r)(1-s)(1+t)W_{ST}+\\(1-r)(1+s)(1-t)W_P+\\(1-r)(1+s)(1+t)W_T+\\(1+r)(1-s)(1-t)W_{SE}+\\(1+r)(1-s)(1+t)W_{SET}+\\(1+r)(1+s)(1-t)W_E+\\(1+r)(1+s)(1+t)W_{ET}\end{pmatrix}}{8} \quad (A.14)$$

And the derivatives can be calculated by the chain rule.

$$\begin{aligned}\frac{\partial W}{\partial x}&=\frac{\partial r}{\partial x}\frac{\partial W}{\partial r}=\frac{2}{\Delta x}\frac{\partial W}{\partial r}\\ \frac{\partial W}{\partial y}&=\frac{\partial s}{\partial y}\frac{\partial W}{\partial s}=\frac{2}{\Delta y}\frac{\partial W}{\partial s}\\ \frac{\partial W}{\partial z}&=\frac{\partial t}{\partial z}\frac{\partial W}{\partial t}=\frac{2}{\Delta z}\frac{\partial W}{\partial t}\end{aligned} \quad (A.15)$$

where Δx, Δy and Δz are length, height and width of the representative cubic element, respectively.Now a relationship between the derivatives of (I_aT_{jk}) at integration points and (I_aT_{jk}) of the nodal points can be obtained by replacing W with (I_aT_{jk}) in Eqs.(A.16) and (A.17). For example at ip=2 (at position (r=0, s=0.5, t= -0.5) in the element of Figure A.1(b)) and ip=12 (at position (r= -0.5, s= -0.5, t=0) in the element of Figure A.1(c))

$$\left.\frac{\partial(I_aT_{11})}{\partial x}\right|_{ip=2}=\frac{\begin{pmatrix}-3(I_aT_{11})_S-(I_aT_{11})_{ST}\\-9(I_aT_{11})_P-3(I_aT_{11})_T\\+3(I_aT_{11})_{SE}+(I_aT_{11})_{SET}\\+9(I_aT_{11})_E+3(I_aT_{11})_{ET}\end{pmatrix}}{16\Delta x}$$

$$\left.\frac{\partial(I_aT_{12})}{\partial y}\right|_{ip=2}=\frac{\begin{pmatrix}-3(I_aT_{12})_S-(I_aT_{12})_{ST}\\+3(I_aT_{12})_P+(I_aT_{12})_T\\-3(I_aT_{12})_{SE}-(I_aT_{12})_{SET}\\+3(I_aT_{12})_E+(I_aT_{12})_{ET}\end{pmatrix}}{8\Delta y}$$

$$\left.\frac{\partial(I_aT_{13})}{\partial z}\right|_{ip=2}=\frac{\begin{pmatrix}-(I_aT_{13})_S+(I_aT_{13})_{ST}\\-3(I_aT_{13})_P+3(I_aT_{13})_T\\-(I_aT_{13})_{SE}+(I_aT_{13})_{SET}\\-3(I_aT_{13})_E+3(I_aT_{13})_{ET}\end{pmatrix}}{8\Delta z}$$

$$\left.\frac{\partial(I_aT_{31})}{\partial x}\right|_{ip=12}=\frac{\begin{pmatrix}-3(I_aT_{31})_P-3(I_aT_{31})_T\\-(I_aT_{31})_N-(I_aT_{31})_{NT}+\\3(I_aT_{31})_E+3(I_aT_{31})_{ET}\\+(I_aT_{31})_{NE}+(I_aT_{31})_{NET}\end{pmatrix}}{8\Delta x} \quad (A.16)$$

$$\left.\frac{\partial(I_aT_{32})}{\partial y}\right|_{ip=12}=\frac{\begin{pmatrix}-3(I_aT_{32})_P-3(I_aT_{32})_T\\+3(I_aT_{32})_N+3(I_aT_{32})_{NT}\\-(I_aT_{32})_E-(I_aT_{32})_{ET}\\+(I_aT_{32})_{NE}+(I_aT_{32})_{NET}\end{pmatrix}}{8\Delta y}$$

$$\left.\frac{\partial(I_aT_{33})}{\partial z}\right|_{ip=12}=\frac{\begin{pmatrix}-9(I_aT_{33})_P+9(I_aT_{33})_T\\-3(I_aT_{33})_N+3(I_aT_{33})_{NT}\\-3(I_aT_{33})_E+3(I_aT_{33})_{ET}\\-(I_aT_{33})_{NE}+(I_aT_{33})_{NET}\end{pmatrix}}{16\Delta z}$$

Considering that there are 24 integration points and similar relations must be derived for each of them and note the fact that different equations must be derived for nodes in the neighborhood of the boundary (because of different configuration of nodal points), the cumbersomeness of coding becomes obvious. A control volume with 6 integration points is shown in Figure A.1(d). Using a central difference scheme for the derivatives, the above formulas for ip=1 simply reduce to

$$\left.\frac{\partial(I_aT_{11})}{\partial x}\right|_{ip=1}=\frac{(I_aT_{11})_E-(I_aT_{11})_P}{\Delta x}$$

$$\left.\frac{\partial(I_aT_{12})}{\partial y}\right|_{ip=1}=0.5\begin{pmatrix}\frac{(I_aT_{12})_{NE}-(I_aT_{12})_{SE}}{\Delta y}\\+\frac{(I_aT_{12})_N-(I_aT_{12})_S}{\Delta y}\end{pmatrix} \quad (A.17)$$

$$\left.\frac{\partial(I_aT_{13})}{\partial z}\right|_{ip=1}=0.5\begin{pmatrix}\frac{(I_aT_{13})_{TE}-(I_aT_{13})_{BE}}{\Delta z}+\\\frac{(I_aT_{13})_T-(I_aT_{13})_B}{\Delta z}\end{pmatrix}$$

which all have a second order of error. Similar relations can be obtained for other integration points of Figure A.1(d) and also for integration points of the elements of 2D and 1D geometries (Figure A.1(e) and Figure A.1(f)). To preserve the order of error in the entire computational domain, additional treatment is needed on the boundary and nodes in its neighborhood. As depicted in Figure A.1(g) for a 2D case, for ip=1

$$\left.\frac{\partial(I_aT_{12})}{\partial y}\right|_{ip=1}=0.5\begin{pmatrix}\frac{4(I_aT_{12})_{NE}-(I_aT_{12})_E-3(I_aT_{12})_{SE}}{3\Delta y}+\\\frac{4(I_aT_{12})_N-(I_aT_{12})_P-3(I_aT_{12})_S}{3\Delta y}\end{pmatrix} \quad (A.18)$$

And for ip=2 where the integration and the northern nodal point coincide

$$(\mathbf{q}\cdot\mathbf{n})\big|_{ip=2}=\varepsilon_{wall}\left(-\sigma T_{wall}^4+I_{a,N}\sum_{X_2^l<0}\alpha^l X_2^l\right) \quad (A.19)$$

Similar equations govern the 3-D case, too.

By replacing the derivatives into Eq. (A.15) one can reach the following equation eventually

$$D_p I_{a,P} = \sum_{nb} D_{nb} I_{a,nb} + B \qquad \text{(A.20)}$$

which is the descretized Q_L equation. The boundary condition for the above equation is

$$I_{a,wall} = \frac{1}{4\pi} \sum_{l=1}^{L} I_{wall}^{l} \Delta\omega^{l} \qquad \text{(A.21)}$$

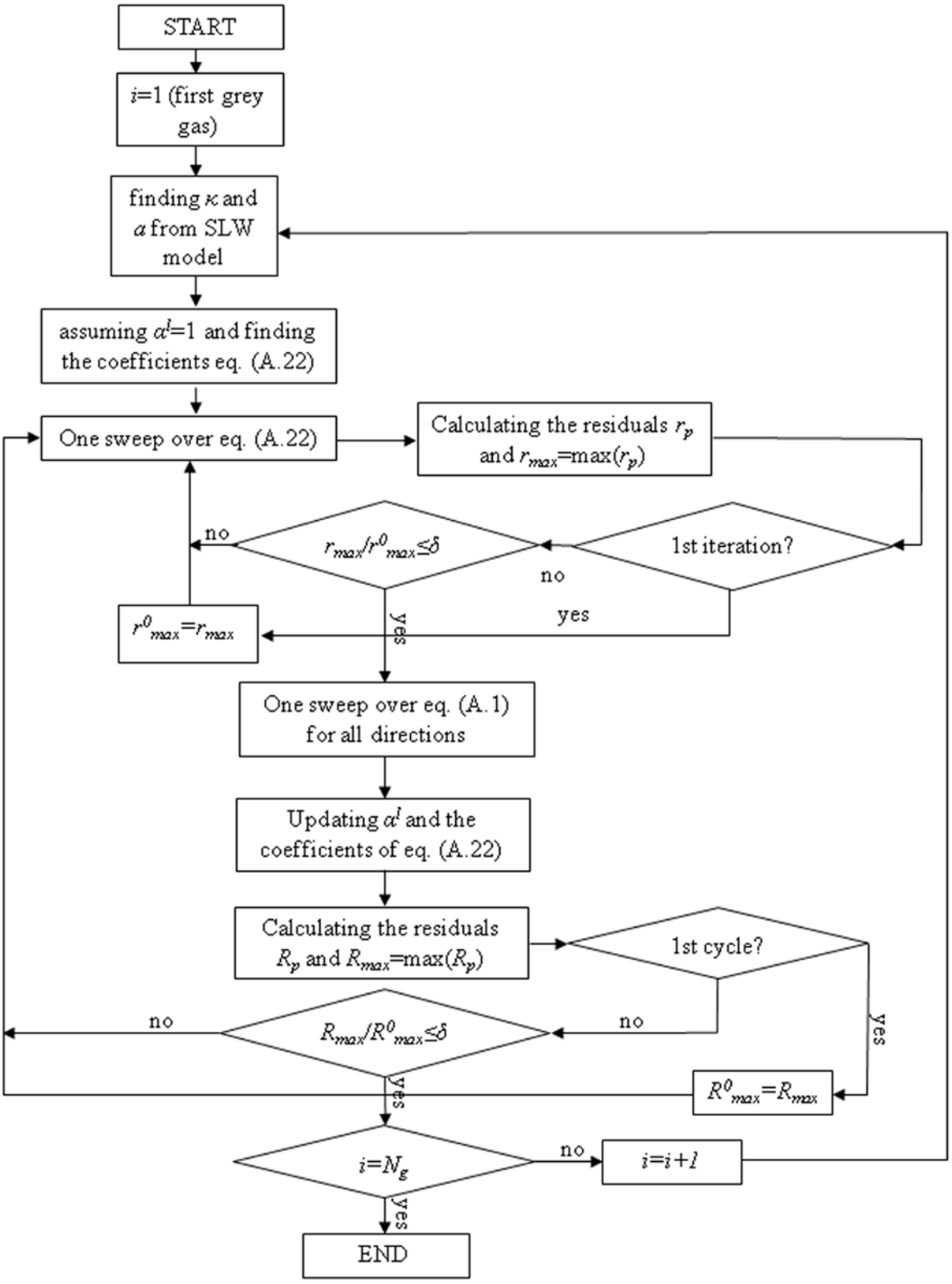

Figure A2. Solution algorithm

The solution algorithm is displayed in Figure A.2 for the case when there is one species in the enclosure. In a short statement it can be said that the directional method produces phase weights (and therefore coefficient of Eq. (A.22)) and boundary condition (Eq. (A.23)). In this study FT*n* FVM with CLAM scheme is used as the directional solver of RTE. Using Eq. (A.22) is proven to increase the convergence rate of solving RTE with a higher accuracy [33].

r_p The scaled residual at each nodal point is [33]

$$r_p = \left| \frac{D_p I_{a,P} - \sum_{nb} D_{nb} I_{a,nb} + B}{D_p \sigma \left(T_g^4 - T_{wall}^4 \right) / \pi} \right| \qquad (A.22)$$

And is calculated at the end of each iteration. R_p is calculated by the same formula but with updated values of D_p, D_{nb} and B. The value of δ is 10^{-5}.

When both H_2O and CO_2 exist in the enclosure, the calculations must be carried out $i=(N_g)^2$ times.

A comparison between the results with different numbers of integration points can be seen in Figure A.3(a) and Figure A.3(b) for the cases of a 2-D enclosure containing grey, emitting and absorbing medium with black cold walls. Also the impact of the number of integration points in 3D cases is studied. First a unit cubical enclosure with diffuse black walls is considered. The radiative equilibrium condition governs the temperature field. Boundaries east (x=1m), south (y=0m) and bottom (z=0m) are hot with E_{bw}=1W/m^2. Other walls are at 0K. The results for G (directionally integrated intensity) are compared with previously published results and shown in Figure A.4(a). Then RTE is solved in an ideal 2m×2m×4m furnace filled with absorbing and emitting medium. The heat source is q'''=5kW/m^3. Boundary conditions are

$$\begin{aligned} &@\, z = 0 : T_w = 1200K \; and \; \varepsilon_w = 0.85 \\ &@\, z = 4m : T_w = 400K \; and \; \varepsilon_w = 0.7 \\ &otherwise \quad T_w = 900K \; and \; \varepsilon_w = 0.7 \end{aligned} \qquad (A.23)$$

The results are shown in Figure A.4(b). The results were similar for other problems (such as scattering media) which are not shown here. It is found that the maximum difference between the results is less than 2% while using one integration point at the center of each face is computationally much cheaper and more compatible with other CFD methods, e.g. FVM. Therefore, for performing calculations in this study, the total number of integration points was selected as 6, 4 and 2 for 3-D, 2-D and 1-D cases, respectively.

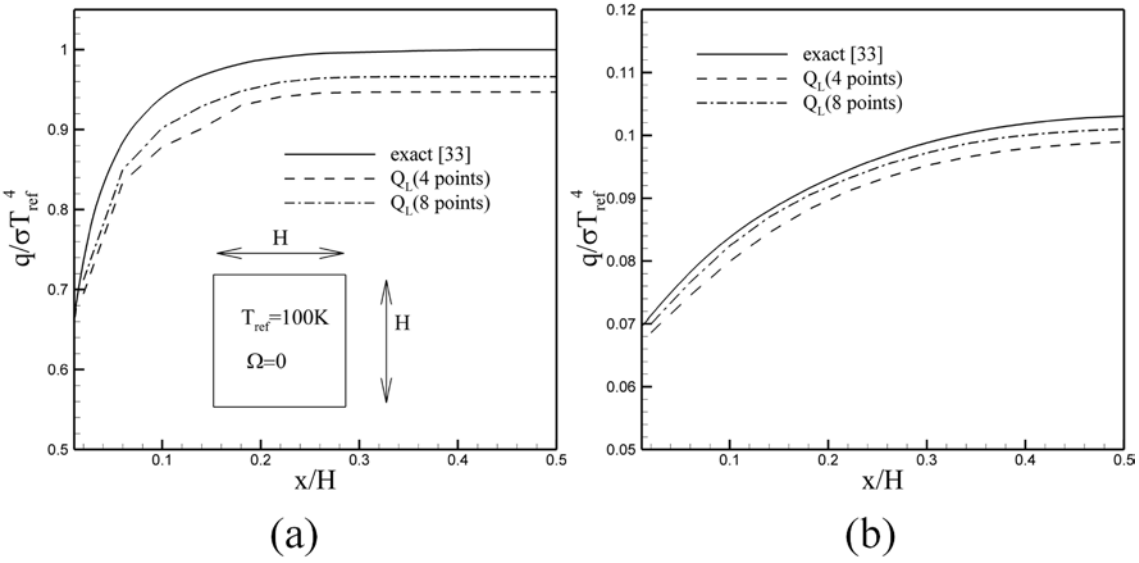

Figure A3. The effect of number of integration points for a 2D problem (a) κH=10 and (b) κH=0.1

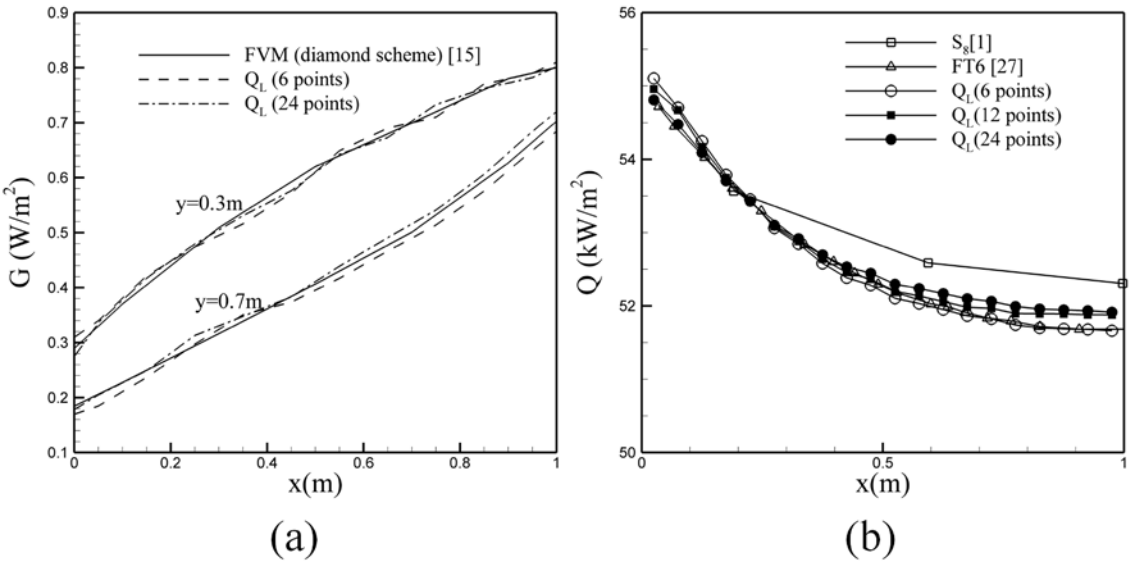

Figure A4. The effect of number of integration points for a 3D problem (a) the incident radiation in a cubic enclosure at z=0.5m (b) the heat flux in an ideal furnace at (x, y=1m, z=2m)